Title

HYPERFINE-STRUCTURE SEPARATIONS, NUCLEAR MAGNETIC MOMENTS, AND HYPERFINE-STRUCTURE ANOMALIES OF GOLD-198 AND GOLD-199

Authors

Bout, Paul A. Vanden
Ehlers, Vernon J.
Niereriberg, William A.
et al.

Publication Date

1966-11-29

UCRL-17297

University of California

Ernest O. Lawrence Radiation Laboratory

HYPERFINE-STRUCTURE SEPARATIONS, NUCLEAR MAGNETIC MOMENTS, AND HYPERFINE-STRUCTURE ANOMALIES OF GOLD-198 AND GOLD-199

DISCLAIMER

To be submitted to Physical Review

UCRL-17297
Preprint

U N I V E R S I T Y O F C A L I F O R N I A

Lawrence Radiation Laboratory
Berkeley, California

AEC Contract No. W-7405-eng-48

HYPERFINE-STRUCTURE SEPARATIONS, NUCLEAR MAGNETIC MOMENTS, AND HYPERFINE-STRUCTURE ANOMALIES OF GOLD-198 AND GOLD-199

Paul A. Vanden Bout, Vernon J. Ehlers, William A. Nierenberg, and Howard A. Shugart

November 29, 1966

UCRL-17297

Hyperfine-Structure Separations, Nuclear Magnetic Moments, and Hyperfine-Structure Anomalies of Gold-198 and Gold-199[†]

Paul A. Vanden Bout, Vernon J. Ehlers,[‡] William A. Nierenberg,[*] and Howard A. Shugart

Department of Physics and Lawrence Radiation Laboratory
University of California, Berkeley, California

November 29, 1966

A B S T R A C T

We have measured the hyperfine-structure separations and nuclear magnetic moments of (2.70 d) Au^{198} and (3.15 d) Au^{199} in the $^2S_{1/2}$ state, using the atomic-beam magnetic-resonance method. We also measured the ratios of the electronic g factor of gold to those of potassium and cesium. The results are, for Au^{198} (I = 2), $\Delta\nu$ = 21450.7167(4) MHz, μ_I(uncorr) = + 0.5842(4) nm; and for Au^{199} (I = 3/2), $\Delta\nu$ = 10962.7227(3) MHz, μ_I(uncorr) = + 0.2673(7) nm. The results for the g-factor ratios are: $g_J(Au)/g_J(K)$ = 1.000504(2) and $g_J(Au)/g_J(Cs)$ = 1.000381(2). These values yield the following hyperfine-structure anomalies: $^{197}\Delta^{198}$ = 8.53(8)% and $^{197}\Delta^{199}$ = 3.7(2)%. Second-order corrections to the hyperfine structure are shown to be negligible. The nuclear results are interpreted in terms of the shell model, with allowance made for configuration mixing.

I. INTRODUCTION

The unpaired s electron present in the atomic $^2S_{1/2}$ ground state of gold is a sensitive probe of the gold nucleus. However, the hyperfine structure (hfs) of this state contains information about only one nuclear multipole moment---the magnetic-dipole moment. Information on higher multipole moments is excluded by angular momentum considerations. Another property, related to the distribution of nuclear magnetism and the electronic wave function, can be measured. This is the hfs anomaly.

The hfs anomaly, $^1\Delta^2$, is defined by:

$$\frac{a_1}{a_2} = \frac{g_1}{g_2}(1 + {}^1\Delta^2) \quad , \tag{1}$$

where the a's are the magnetic-dipole hfs interaction constants, and the g's are the nuclear g factors of isotopes 1 and 2 of the same element. Usually Δ is expressed as a percent and, by convention, isotope 1 is lighter than isotope 2. Part of the origin of the hfs anomaly was explained by Bohr and Weisskopf as arising from the different distributions of magnetism within the nuclei of the two isotopes.[1] The other part, treated by Rosenthal and Breit, arises from the altered electronic wave function in different isotopes.[2] We expected to observe large hfs anomalies in gold because of the large density of electrons at the nucleus and because of the differing spin and orbital contributions to the magnetic-dipole moments of the isotopes.

The Hamiltonian describing the (J = 1/2) ground-state hyperfine structure of gold is

$$\mathcal{H} = ha\,\underset{\sim}{I}\cdot\underset{\sim}{J} - g_I\,\mu_0\,\underset{\sim}{I}\cdot\underset{\sim}{H} - g_J\,\mu_0\,\underset{\sim}{J}\cdot\underset{\sim}{H}\ , \qquad (2)$$

where $\underset{\sim}{I}$ is the nuclear angular momentum, $\underset{\sim}{J}$ is the electronic angular momentum, g_I and g_J are the corresponding g factors, $\underset{\sim}{H}$ is the applied magnetic field, μ_0 is the Bohr magneton, and h is Planck's constant. Precision measurements of transition frequencies between the energy eigenstates of this Hamiltonian yield values of a, g_I, and g_J. It is then possible to calculate Δ using Eq. (1). We made the measurements with an atomic-beam apparatus, inducing the transitions with a radio-frequency (rf) magnetic field.

The experimental results for Au^{198} and Au^{199} are not obviously predicted by calculations based on any single current nuclear model. We have resorted to a fitting scheme, using a configuration-mixing theory to discuss our results.[3] Configuration-mixing theory uses single-particle wave functions admixed with nearby configurations in the calculation of the matrix elements yielding μ_I and Δ. Stroke *et al.* tabulate these matrix elements for a large number of admixtures and isotopes.[4]

II. EXPERIMENTAL METHOD AND APPARATUS

The energy levels of Eq. (2), for J = 1/2, are given by the Breit-Rabi formula

$$W(F, m_F) = \frac{h\Delta\nu}{2(2I+1)} - g_I\,\mu_0\,H\,m_F + (F-I)\,h\Delta\nu\left\{1 + \frac{4\,m_F x}{2I+1} + x^2\right\}^{1/2}\ , \qquad (3)$$

where $\Delta\nu = a(I + \tfrac{1}{2})$ and $x = (g_I - g_J)\,H(\mu_0/h)$. The energy levels for Au^{198} and Au^{199} as a function of magnetic field H are given in Figs. 1 and 2, respectively.

The operation of a flop-in atomic-beam apparatus has been described in great detail elsewhere;[5] we will give only a brief description here. Atoms effuse from an oven and travel essentially collision-free through a strongly inhomogeneous A magnet, a very homogeneous C magnet, and a strongly inhomogeneous B magnet. Because they have a magnetic-dipole moment of approximately one Bohr magneton, the atoms are deflected in the inhomogeneous fields. For a beam of atoms with $J = 1/2$, these deflections in the A and B fields will cancel and a signal will be seen at the detector if atomic transitions are induced in the C field for which $\Delta m_J = \pm 1$. In this experiment the magnetic field H was held constant and the frequency ν was varied; the observed signal exhibited a resonant behavior as a function of ν. The magnetic field was measured by observing the standard $\Delta F = 0$ transition in either K^{39} or Cs^{133}.

The distinguishing feature of our apparatus is its C magnet. The magnet (Varian V4012A) has 12-inch pole tips with a 2-inch gap. This allows for considerable flexibility in the choice and use of rf loops. The magnet is capable of producing fields up to 10,000 G. As an indication of the magnets' homogeneity, the standard $\Delta F = 0$ transition in K^{39} has typically a full-width at half-maximum of 100 kHz at 4500 G using a hairpin 1 cm long.

The A and B magnets, which operate with a gradient of approximately 10,000 G/cm, are identical, making the machine symmetric about the C magnet. The oven-detector distance is about 270 cm. The apparatus is divided into chambers which are differentially pumped by oil diffusion pumps. With the exception of the oven chamber, the pressures achieved are less than 1.0×10^{-6} mm Hg.

Gold-198 was produced by thermal neutron irradiation of 100% Au^{197}. About 0.1 g of small gold chips were irradiated for 16 hours in a 10^{14} neutrons per cm^2-sec flux. These chips were placed directly in the oven. To produce Au^{199}, about 2.5 g of Pt were irradiated in a 10^{14} neutrons per cm^2-sec flux for 48 hours. The Pt^{199} thus produced decayed with a half-life of 30 minutes to Au^{199}. A standard ethyl acetate separation removed the Au^{199} together with some Au^{197} carrier from an *aqua regia* solution of the Pt.

We used a tantalum oven heated by electron bombardment to produce beams. Because gold and tantalum form an alloy at high temperatures, the oven was fitted with an inner liner and a snout, both made of carbon. Beams of stable alkali atoms, used in calibrating the magnetic field, were obtained from a resistance-heated stainless steel oven.

The radioactive beams were detected by collecting them on a sulfur surface for five minutes and then placing this surface in an anti-coincidence shielded Geiger counter where they were counted. Alkali beams were detected by ionizing them with a hot iridium wire and measuring the ion current.

When the experiment began, we knew the nuclear spins and had preliminary values for the $\Delta\nu$'s from the work of Christensen *et al.*[6] Our first measurements for both isotopes of gold consisted of a series of observations of the standard $\Delta F = 0$ transition at increasingly higher magnetic fields. This provided values of a and g_I sufficiently precise to allow a search for a $\Delta F = 1$ transition. The $\Delta F = 0$ transition also determined g_J. For these measurements the "hairpins" or rf loops

illustrated in Fig. 3 were used, the one on the left for low frequencies and the one on the right for high frequencies. The hairpin terminating in the 50-ohm load was required at high fields (> 1000 G) to avoid inconsistencies in the magnetic-field calibration. These occur at high fields with the shorted hairpin because the rf power at the gold frequency maximized at a different location in the hairpin than the location of the maximum rf power for the alkali frequency. Due to magnetic field inhomogeneities, the two resonances occurred in different fields, thus causing a systematic error when a comparison is made. The magnetic field was regulated during these measurements to a few parts per million by a nuclear magnetic-resonance feedback circuit. The rf signal sources were either frequency synthesizers (Schomandl FD3) followed by amplifiers, or klystrons phase-locked to a frequency synthesizer.

To determine $\Delta\nu$, we observed the $(5/2, \pm 1/2) \leftrightarrow (3/2, \mp 1/2)$ transition in Au^{198} and the $(2,0) \leftrightarrow (1,0)$ transition in Au^{199}. At zero magnetic field the frequencies of these transitions do not depend to first order on the magnetic field. Hence, inhomogeneity-produced line broadening is small, and narrow lines are possible.

The final observations of these lines were made with cavity hairpins. The coaxial hairpin shown in Fig. 4 was used to calibrate the magnetic field. The entire hairpin block could be moved to allow either hairpin to occupy the center of the C magnet. For Au^{198} the cavity operated in the TE_{011} mode; for Au^{199} the TM_{010} mode was used. Observations were made with various orientations of cavity and C-field directions to check for cavity shifts and Millman effects.[7] None were observed. During all of these final

observations we varied the rf power at the peak frequency to determine the optimum transition power. The cavity hairpins typically required a few microwatts of rf power to saturate the resonance.

To determine g_I, the doublets were observed at their field-independent points. In Au^{198} these are the transitions (5/2, -3/2) ↔ (3/2, - 1/2) and (5/2, -1/2) ↔ (3/2, -3/2) at 3200 G; in Au^{199} these are the transitions (2, -1) ↔ (1, 0) and (2, 0) ↔ (1, -1) at 1040 G. Again, cavity hairpins operating in the same modes as those for the $\Delta\nu$ measurements were used. Millman or cavity shifts were also not observed for these transitions.

All frequency counters and rf equipment used in this experiment had as a reference a 100-kHz oscillator (James Knight FS1100T). This oscillator was continuously monitored against the standard 60-kHz WWVB broadcasts. Therefore, all our measurements of frequency are based on atomic time A 1 which defines the second by taking the $\Delta\nu$ of Cs^{133} to be 9192.631770 MHz exactly.

III. DATA AND RESULTS

The data for Au^{198} and Au^{199} are presented in Tables I and II, respectively. The residuals listed there are the calculated frequencies, based on the best least-squares fit, minus the experimentally observed frequencies. Figures 5 through 8 illustrate typical observed resonances. These data were fitted to the Breit-Rabi formula using a least-squares fitting routine. The parameters g_I, g_J, and a were varied and the results are given in Table III. The value μ_0/h = 1.399613 MHz/G was used in this fitting routine. The results do not depend on this value to first order because of the method of measuring the magnetic field. Table IV gives the constants assumed for the calibration isotopes used to calculate the magnetic field.

The final experimental results, which supersede all prior information,[8] are listed in Table V. The value $m_p/m_e = 1836.12$ was used to calculate the nuclear magnetic moments, and the correction for diamagnetism[9] was taken to be $(1-\sigma)^{-1} = 1.00958$. The results for the ratios of the electronic g_J factors, as well as the other results, are quite independent of the absolute value taken for the alkali g_J factors. A variation of 1 part in 10^5 can easily be tolerated.

Our final results have errors representing 2 standard deviations of the least-squares fit based on external consistency of the input data. The resulting χ^2's indicate that our choice of input uncertainties was highly conservative, but these choices reflect considerations of possible systematic errors. The hyperfine-structure anomalies were calculated with the following values[10] for Au^{197}:

$$\Delta\nu = 6099.320184(13) \text{ MHz}$$

$$\mu_I \text{ (uncorr)} = + 0.143491(9) \text{ nm} \quad .$$

IV. DISCUSSION

We have considered the effect on our results of second-order contributions to the hyperfine structure. All such matrix elements of Eq. (2) which are off-diagonal in J, and which also involve the magnetic field H, vanish identically. This is because they all contain the integral

$$\int R_{6s}\, R_{n\ell}\, dr$$

as a factor in their reduced matrix elements. One of the selection rules on this integral is $\Delta n = 0$. Because the ground-state configuration of gold

leads to only one fine-structure level, this integral vanishes. Hence, the Breit-Rabi formula yields the true g_I and g_J.

We have calculated the second-order magnetic-dipole and electric-quadrupole contributions to the ground-state hyperfine structure from the $^2D_{3/2}$ and $^2D_{5/2}$ states, following Schwartz.[11] The results of Childs and Goodman[12] for the hyperfine structure of these states in Au^{197} were used to determine the normalization of the Casimir wave functions. If we set the experimental $\Delta\nu$ equal to $\Delta\nu_{\text{1st order}} + \Delta\nu_{\text{2nd order}}$, then $\Delta\nu_{\text{2nd order}}\ (Au^{198}) = -34.$ Hz, $\Delta\nu_{\text{2nd order}}\ (Au^{199}) = -68.$ Hz . In these calculations we have assumed that the nuclear electric-quadrupole moments of these isotopes are no larger than 1 barn. These corrections are negligible for present measurements.

The spin of Au^{199} is 3/2, as is the spin of all the odd-A gold isotopes. The most reasonable explanation is that these spins are due to the $d_{3/2}$ hole in the proton configuration $(1g_{7/2})^8\ (2d_{5/2})^6\ (1h_{11/2})^{12}\ (2d_{3/2})^3$, where only states above the closed shell at 50 protons are listed. This assignment of the $2d_{3/2}$ protons is consistent with the observed positive nuclear quadrupole moment of Au^{197} (Ref. 12). It is also consistent with the fact that the observed moment is closest to the Schmidt moment corresponding to $j = \ell - 1/2$.

If the odd neutron in Au^{198} is assumed to be in a $3p_{1/2}$ state, then Nordheim's rules as modified by Brennen and Bernstein[13] unambiguously predict that the spin is 2. This is indeed the observed spin. This neutron assignment is also consistent with the observed spin and parity[14] of Hg^{199}.

The Schmidt predictions for the magnetic moments are: $\mu_I(Au^{199}) = +0.124$ nm, and $\mu_I(Au^{198}) = +0.762$ nm. No nuclear model known to us can explain the deviation of the observed moments from these values and at the same time predict the observed anomalies.

In view of the difficulties of theoretically predicting the magnetic moments, we construct an interpretation of the observed moments by the following scheme. The theoretical magnetic moments of Au^{197} and Au^{199} are made to fit the observed moments either by choosing the proper value of g_s in the Schmidt formula (the method of quenched g factors) or by choosing the proper admixture of some single-excitation configuration-mixing scheme. For each value of g_s and admixture, a value of ϵ can be calculated. The single-isotope anomaly (ϵ) is defined by $a_{ext} = a_{pt}(1 + \epsilon)$, where a_{ext} and a_{pt} are the hfs interaction constants calculated with a distribution of nuclear magnetism and a point magnetic dipole, respectively. The hyperfine-structure anomaly is then calculated using

$$1 + {}^1\Delta^2 = \frac{1 + \epsilon_1}{1 + \epsilon_2} \quad . \tag{4}$$

The scheme which then predicts the best values of ${}^{197}\Delta^{199}$ is chosen as best describing the observed facts. Table VI gives the results of this calculation for ${}^{197}\Delta^{199}$.

It is easily seen that the use of effective g_s factors leads to a poor value for the anomaly. Both neutron excitations give reasonable agreement, and we choose $(p_{1/2} - p_{3/2})$ as best describing the situation since it has the lower excitation energy.

The magnetic-dipole moment of Au^{198} can be calculated using the g factor of the neutron in Hg^{199} and the g factor of the proton in either

Au^{197} or Au^{199}. We use the value $\mu_I = +0.50$ nm for the magnetic moment[14] of Hg^{199}. Taking the proton g factor from Au^{197}, we get $\mu_I(Au^{198}) = +0.65$ nm, and using the proton g factor from Au^{199}, we get $\mu_I(Au^{198}) = +0.77$ nm. Although neither value agrees very well with the observed value of +0.59 nm, this is probably as good as can be expected for an odd-odd nucleus.

A value of ε for Au^{198} can be calculated from

$$\varepsilon = \alpha_p \varepsilon_p + \alpha_n \varepsilon_n , \qquad (5)$$

where α_p and α_n are the fractional contributions of the proton and the neutron to the magnetic moment of Au^{198}, respectively, and ε_p and ε_n are the values of the individual isotope hfs anomaly for the proton and neutron alone.[15] For ε_p we can choose either $\varepsilon(Au^{197}) = 13.6\%$ or $\varepsilon(Au^{199}) = 8.3\%$, and for ε_n we use $\varepsilon(Hg^{199}) = -3.5\%$. The delta function interaction assumed in Refs. 2 and 3 to cause the configuration mixing vanishes for the single $p_{1/2}$ neutron in Hg^{199}. Therefore, an effective g factor is used in calculating $\varepsilon(Hg^{199})$. Using $\varepsilon(Au^{197})$ and $\varepsilon(Hg^{199})$, we get $\varepsilon(Au^{198}) = 0.89\%$, with $^{197}\Delta^{198} = 12.6\%$; using $\varepsilon(Au^{199})$ and $\varepsilon(Hg^{199})$, we get $\varepsilon(Au^{198}) = 2.7\%$, with $^{197}\Delta^{198} = 10.6\%$. The second case gives reasonable agreement with the observed value of $^{197}\Delta^{198} = 8.5\%$.

V. CONCLUSIONS

As expected, the hfs anomalies $^{197}\Delta^{198}$ and $^{197}\Delta^{199}$ are large. We have shown that the hfs anomaly is not necessarily a "1% effect" as it is often labeled. Its usefulness as a nuclear parameter is limited because of the complexity of its interpretation. However, it can be helpful when we are deciding among several possible fitting schemes in which configuration mixing is being used to explain a magnetic moment. By such a scheme, we have

attempted to explain the magnetic-dipole moments of Au^{198} and Au^{199} and their anomalies with respect to Au^{197}.

REFERENCES

† Supported in part by the U. S. Atomic Energy Commission and in part by the National Science Foundation.

‡ Present address: Calvin College, Grand Rapids, Michigan.

* Present address: Scripps Institution of Oceanography, University of California, San Diego.

1. Aage Bohr and V. F. Weisskopf, Phys. Rev. 77, 94 (1950).
2. Jenny E. Rosenthal and G. Breit, Phys. Rev. 41, 459 (1932).
3. Akito Arima and Hisashi Horie, Progr. Theoret. Phys. (Kyoto) 12, 623 (1954).
4. H. H. Stroke, R. J. Blin-Stoyle, and V. Jaccarino, Phys. Rev. 123, 1326 (1961).
5. Norman F. Ramsey, Molecular Beams (Oxford University Press, 1956); Hans Kopferman, Nuclear Moments (Academic Press, Inc., New York, N.Y., 1958).
6. R. L. Christensen, D. R. Hamilton, A. Lemonick, F. M. Pipkin, J. B. Reynolds, and H. H. Stroke, Phys. Rev. 101, 1389 (1956).
7. S. Millman, Phys. Rev. 55, 628 (1939).
8. P. A. Vanden Bout, V. J. Ehlers, W. A. Nierenberg, and M. H. Prior, Bull. Am. Phys. Soc. 8, 619 (1963); P. A. Vanden Bout, V. J. Ehlers, and W. A. Nierenberg, Bull. Am. Phys. Soc. 10, 691 (1965); P. A. Vanden Bout, V. J. Ehlers, W. A. Nierenberg, and H. A. Shugart, Bull. Am. Phys. Soc. 11, 343 (1966).
9. W. C. Dickinson, Phys. Rev. 80, 563 (1950).

10. S. Penselin (Physikalisches Institut der Universität, Bonn, Germany) personal communication, 1963.

11. Charles Schwartz, Phys. Rev. 97, 380 (1955); and Phys. Rev. 105, 173 (1957).

12. W. J. Childs and L. S. Goodman, Phys. Rev. 141, 176 (1966).

13. M. H. Brennan and A. M. Bernstein, Phys. Rev. 120, 927 (1960).

14. Bernard Cagnac, Ann. Phys. (Paris) 6, 467 (1961).

15. Norman Braslau, Gilbert O. Brink, and Jhan Khan, Phys. Rev. 123, 1801 (1961); and S. Schmelling (to be published in Phys. Rev.).

Table I. Experimental data for Au^{198}.

Run	Calib. isotope	$\nu_{calib.}$ (MHz)	H(G)	Gold transition $(F_1, m_1) - (F_2, m_2)$	ν_{Au} (MHz)	Residual
4A	K^{39}	44.2149(55)	50.0058(50)	(5/2, -3/2)-(5/2, -5/2)	28.1840(50)	+ 0.0039
4B	K^{39}	200.5925(75)	150.0154(37)	(5/2, -3/2)-(5/2, -5/2)	85.4300(35)	- 0.0030
4C	K^{39}	684.5815(55)	350.0205(21)	(5/2, -3/2)-(5/2, -5/2)	203.6012(35)	- 0.0031
4D	K^{39}	2750.4857(70)	1100.0523(25)	(5/2, -3/2)-(5/2, -5/2)	694.0465(45)	- 0.0022
8H	Cs^{133}	1947.397(13)	2500.1548(88)	(5/2, -3/2)-(5/2, -5/2)	1846.123(10)	- 0.0064
8I	Cs^{133}	1947.391(13)	2500.1509(88)	(5/2, -3/2)-(5/2, -5/2)	1846.115(8)	- 0.0106
32A	Cs^{133}	0.5441(70)	1.554(20)	(5/2, 1/2)-(3/2, 1/2)	21451.585(13)	- 0.0040
32B	Cs^{133}	0.6030(70)	1.723(20)	(5/2, 1/2)-(3/2, -1/2)	21450.720(26)	+ 0.0031
32C1	Cs^{133}	6119.922(18)	4599.8575(75)	(5/2, -3/2)-(5/2, -5/2)	4303.085(14)	- 0.0032
32C2	Cs^{133}	6119.913(18)	4599.8538(75)	(5/2, -3/2)-(5/2, -5/2)	4303.087(12)	+ 0.0039
32D1	Cs^{133}	6119.906(18)	4599.8507(75)	(5/2, -3/2)-(5/2, -5/2)	4303.083(12)	+ 0.0043
32D2	Cs^{133}	6119.901(18)	4599.8485(75)	(5/2, -3/2)-(5/2, -5/2)	4303.082(12)	+ 0.0063
32F1	Cs^{133}	11998.303(24)	6899.9470(90)	(5/2, -3/2)-(5/2, -5/2)	8118.300(24)	+ 0.0082
32F2	Cs^{133}	11998.328(24)	6899.9564(90)	(5/2, -3/2)-(5/2, -5/2)	8118.310(24)	+ 0.0004
32F3	Cs^{133}	11998.323(24)	6899.9545(90)	(5/2, -3/2)-(5/2, -5/2)	8118.305(24)	- 0.0011
37A1	Cs^{133}	3126.650(10)	3214.4648(54)	(5/2, -1/2)-(3/2, -3/2)	19564.390(30)	+ 0.0017
37A2	Cs^{133}	3126.656(10)	3214.4680(54)	(5/2, -1/2)-(3/2, -3/2)	19564.390(30)	+ 0.0017
37A3	Cs^{133}	3126.657(10)	3214.4684(54)	(5/2, -1/2)-(3/2, -3/2)	19564.390(30)	+ 0.0017
37B1	Cs^{133}	3126.632(10)	3214.4552(54)	(5/2, -3/2)-(3/2, -1/2)	19565.820(30)	+ 0.0002
37B2	Cs^{133}	3126.633(10)	3214.4558(54)	(5/2, -3/2)-(3/2, -1/2)	19565.820(30)	+ 0.0002
37B3	Cs^{133}	3126.636(10)	3214.4573(54)	(5/2, -3/2)-(3/2, -1/2)	19565.820(30)	+ 0.0002
37C1	Cs^{133}	3126.655(10)	3214.4675(54)	(5/2, -1/2)-(3/2, -3/2)	19564.390(30)	+ 0.0017
37C2	Cs^{133}	3126.655(10)	3214.4675(54)	(5/2, -1/2)-(3/2, -3/2)	19564.390(30)	+ 0.0017
37C3	Cs^{133}	3126.655(10)	3214.4675(54)	(5/2, -1/2)-(3/2, -3/2)	19564.390(30)	+ 0.0017
37C4	Cs^{133}	3126.639(10)	3214.4590(54)	(5/2, -3/2)-(3/2, -1/2)	19565.820(30)	+ 0.0002
37C5	Cs^{133}	3126.639(10)	3214.4590(54)	(5/2, -3/2)-(3/2, -1/2)	19565.820(30)	+ 0.0002
37C6	Cs^{133}	3126.639(10)	3214.4590(54)	(5/2, -3/2)-(3/2, -1/2)	19565.820(30)	+ 0.0002
47A1	Cs^{133}	3126.684(17)	3214.4829(91)	(5/2, -3/2)-(3/2, -1/2)	19565.8202(27)	+ 0.0004
47A2	Cs^{133}	3126.712(17)	3214.4979(91)	(5/2, -3/2)-(3/2, -1/2)	19565.8202(25)	+ 0.0004
47B1	Cs^{133}	3126.659(35)	3214.470(19)	(5/2, -1/2)-(3/2, -3/2)	19564.3877(25)	- 0.0006
47B2	Cs^{133}	3126.662(35)	3214.471(19)	(5/2, -1/2)-(3/2, -3/2)	19564.3877(25)	- 0.0006
50A1	Cs^{133}	3126.7240(60)	3214.5046(32)	(5/2, -3/2)-(3/2, -1/2)	19565.8198(7)	+ 0.0000
50A2	Cs^{133}	3126.7240(60)	3214.5046(32)	(5/2, -3/2)-(3/2, -1/2)	19565.8198(8)	+ 0.0000
50A3	Cs^{133}	3126.7250(60)	3214.5052(32)	(5/2, -1/2)-(3/2, -3/2)	19564.3885(7)	+ 0.0002
50A4	Cs^{133}	3126.7250(60)	3214.5052(32)	(5/2, -1/2)-(3/2, -3/2)	19564.3885(7)	+ 0.0002
50B1	Cs^{133}	3126.7290(60)	3214.5073(32)	(5/2, -1/2)-(3/2, -3/2)	19564.3885(7)	+ 0.0002
50B2	Cs^{133}	3126.7290(60)	3214.5073(32)	(5/2, -3/2)-(3/2, -1/2)	19565.8198(8)	+ 0.0000
50B3	Cs^{133}	3126.7200(60)	3214.5025(32)	(5/2, -3/2)-(3/2, -1/2)	19565.8196(8)	- 0.0002
50B4	Cs^{133}	3126.7220(60)	3214.5036(32)	(5/2, -1/2)-(3/2, -3/2)	19564.3879(7)	- 0.0004
50B5	Cs^{133}	0.310(10)	0.886(29)	(5/2, -1/2)-(3/2, 1/2)	21450.7173(9)	+ 0.0002
50B5	Cs^{133}	0.310(10)	0.886(29)	(5/2, 1/2)-(3/2, -1/2)	21450.7173(9)	+ 0.0006
50B6	Cs^{133}	0.310(10)	0.886(29)	(5/2, -1/2)-(3/2, 1/2)	21450.7169(9)	- 0.0002
50B6	Cs^{133}	0.310(10)	0.886(29)	(5/2, 1/2)-(3/2, -1/2)	21450.7169(9)	+ 0.0002
50C1	Cs^{133}	0.315(10)	0.900(29)	(5/2, -1/2)-(3/2, 1/2)	21450.7164(12)	- 0.0007
50C1	Cs^{133}	0.315(10)	0.900(29)	(5/2, 1/2)-(3/2, -1/2)	21450.7164(12)	- 0.0003
50C2	Cs^{133}	0.286(10)	0.817(29)	(5/2, -1/2)-(3/2, 1/2)	21450.7168(10)	- 0.0002
50C2	Cs^{133}	0.286(10)	0.817(29)	(5/2, 1/2)-(3/2, -1/2)	21450.7168(10)	+ 0.0001

Table II. Experimental data for Au^{199}.

Run	Calib. isotope	$\nu_{calib.}$ (MHz)	H(G)	Gold transition $(F_1, m_1)-(F_2, m_2)$	ν_{Au} (MHz)	Residual
6A	K^{39}	44.2092(75)	50.0006(68)	(2, -1)-(2, -2)	35.3835(75)	+ 0.0017
6B	K^{39}	200.5910(75)	150.0146(37)	(2, -1)-(2, -2)	108.2210(60)	- 0.0029
6C	K^{39}	503.0970(85)	280.0303(3)	(2, -1)-(2, -2)	207.1910(40)	- 0.0035
6D	K^{39}	2750.4095(85)	1100.0250(30)	(2, -1)-(2, -2)	956.658(10)	- 0.0044
10A	Cs^{133}	500.4140(75)	1049.890(12)	(2, 0)-(1, -1)	10589.038(13)	+ 0.0014
10B	Cs^{133}	500.4140(75)	1049.890(12)	(2, 0)-(1, -1)	10589.0396(40)	+ 0.0035
10C	Cs^{133}	500.4140(75)	1049.890(12)	(2, -1)-(1, 0)	10589.3191(90)	- 0.0023
10D	Cs^{133}	500.4140(75)	1049.890(12)	(2, -1)-(1, 0)	10589.3216(50)	+ 0.0002
13A	K^{39}	0.7051(70)	1.0020(99)	(2, -1)-(1, 0)	10962.0255(90)	+ 0.0048
13B	K^{39}	0.7042(65)	1.0008(92)	(2, -1)-(1, 0)	10962.0240(60)	+ 0.0024
13C	K^{39}	0.7035(70)	0.9998(99)	(2, 0)-(1, 0)	10962.7215(90)	- 0.0015
13D	K^{39}	0.7026(70)	0.9985(99)	(2, 0)-(1, 0)	10962.723(10)	- 0.0005
13G	Cs^{133}	498.9456(80)	1047.584(13)	(2, -1)-(1, 0)	10589.3185(40)	- 0.000
13H	Cs^{133}	498.9480(80)	1047.588(13)	(2, -1)-(1, 0)	10589.3187(55)	- 0.0006
13I	Cs^{133}	498.9500(80)	1047.591(13)	(2, 0)-(1, -1)	10589.0360(70)	+ 0.0014
13J	Cs^{133}	498.9528(80)	1047.595(13)	(2, 0)-(1, -1)	10589.0368(30)	+ 0.0022
26A	K^{39}	5546.432(10)	2100.1932(36)	(2, -1)-(2, -2)	2214.1790(80)	- 0.0000
26A	K^{39}	5546.343(10)	2100.1614(36)	(2, -1)-(2, -2)	2214.1350(60)	+ 0.0025
26B	K^{39}	8627.052(12)	3200.3448(43)	(2, -1)-(2, -2)	4063.048(10)	+ 0.0057
26D	Cs^{133}	8345.833(15)	5500.3416(59)	(2, -1)-(2, -2)	9102.635(15)	- 0.0091
26E	Cs^{133}	11468.376(25)	6700.3448(94)	(2, -1)-(2, -2)	12084.595(24)	- 0.0013
46A1	Cs^{133}	498.9408(70)	1047.577(11)	(2, 0)-(1, -1)	10589.0345(10)	- 0.0001
46A2	Cs^{133}	498.9324(70)	1047.563(11)	(2, 0)-(1, -1)	10589.0357(12)	+ 0.0011
46B1	Cs^{133}	498.9296(70)	1047.559(11)	(2, -1)-(1, 0)	10589.3195(13)	+ 0.0002
46B2	Cs^{133}	498.9503(70)	1047.592(11)	(2, -1)-(1, 0)	10589.3195(12)	+ 0.0002
49B1	Cs^{133}	498.9430(60)	1047.5801(94)	(2, 0)-(1, -1)	10589.0345(5)	- 0.0001
49B2	Cs^{133}	498.9440(60)	1047.5816(94)	(2, 0)-(1, -1)	10589.0345(8)	- 0.0001
49B3	Cs^{133}	498.9550(60)	1047.5989(94)	(2, 0)-(1, -1)	10589.0345(6)	- 0.0001
49B4	Cs^{133}	498.9610(60)	1047.6083(94)	(2, 0)-(1, -1)	10589.0345(4)	- 0.0001
49B5	Cs^{133}	498.9440(60)	1047.5816(94)	(2, -1)-(1, 0)	10589.3192(5)	- 0.0001
49B6	Cs^{133}	498.9450(60)	1047.5832(94)	(2, -1)-(1, 0)	10589.3192(6)	- 0.0001
49B7	Cs^{133}	498.9530(60)	1047.5958(94)	(2, -1)-(1, 0)	10589.3192(8)	- 0.0001
49B8	Cs^{133}	498.9630(60)	1047.6115(94)	(2, -1)-(1, 0)	10589.3192(4)	- 0.0001
49C1	Cs^{133}	0.265(10)	0.757(29)	(2, 0)-(1, 0)	10962.7231(4)	+ 0.0002
49C2	Cs^{133}	0.267(10)	0.763(29)	(2, 0)-(1, 0)	10962.7227(4)	- 0.0002
49C3	Cs^{133}	0.269(10)	0.769(29)	(2, 0)-(1, 0)	10962.7229(5)	+ 0.0000
49C4	Cs^{133}	0.302(10)	0.863(29)	(2, 0)-(1, 0)	10962.7231(6)	+ 0.0002

Table III. Results of least-squares fit.

	Au^{198} (I = 2)	Au^{199} (I = 3/2)
a	8580.286697(87) MHz	5481.361327(71) MHz
g_I (uncorr)	+ 0.000159084(57)	+ 0.00009706(12)
g_J	- 2.0033055(17)	- 2.0033037(19)
Number of observations	47	37
χ^2	5.4	4.9

Table IV. Calibration isotope constants.

	K^{39}	Cs^{133}
$\Delta\nu$	461.719723[a] MHz	9192.631770[b] MHz
μ_I (uncorr)	+ 0.39088[c] nm	+ 2.5641[c] nm
g_J	- 2.0022954[d]	- 2.0025417[d]

a. Reference 10.

b. Atomic time, A1, defines the second by assuming this $\Delta\nu$ for Cs^{133}.

c. Ingvar Lindgren, Table of Nuclear Spins and Moments, in Alpha-, Beta-, and Gamma-Ray Spectroscopy, Vol. 2, Kai Siegbahn, Ed., (North-Holland Publ. Co., Amsterdam, 1965) p. 1621.

d. P. A. Vanden Bout, V. J. Ehlers, and T. Incesu, Bull. Am. Phys. Soc. 9, 740 (1964); L. C. Balling and F. M. Pipkin, Phys. Rev. 139, A19 (1965); and D. T. Wilkinson and H. R. Crane, Phys. Rev. 130, 852 (1963).

Table V. Final results.

	Au^{198} (I = 2)	Au^{199} (I = 3/2)
$\Delta\nu$	21450.7167(4) MHz	10962.7227(3) MHz
μ_I (uncorr)	+ 0.5842(4) nm	+ 0.2673(7) nm
μ_I (corr)	+ 0.5898(4) nm	+ 0.2699(7) nm
$^{197}\Delta$---	8.53(8)%	3.7(2)%

$$g_J(Au^{198,199})/g_J(K^{39}) = 1.000504(2)$$

$$g_J(Au^{198,199})/g_J(Cs^{133}) = 1.000381(2)$$

Table VI. Interpretation of Au^{199} result.

Mechanism	Excitation energy (MeV)	$\varepsilon(Au^{197})$	$\varepsilon(Au^{199})$	$^{197}\Delta^{199}$ [a]
effective g_s	---	13.0	4.9	7.7
$\nu(p_{1/2} - p_{3/2})$	0.5	13.6	8.3	4.9
$\nu(i_{11/2} - i_{13/2})$	2.0	13.7	8.4	4.9
$\pi(h_{9/2} - h_{11/2})$	2.0	13.1	6.1	6.6
$\pi(d_{3/2} - d_{5/2})$	1.5	13.1	6.4	6.4

a. Experimentally, $^{197}\Delta^{199}$ = 3.7(2)% .

FIGURE CAPTIONS

Fig. 1. Breit-Rabi diagram for Au^{198} (I = 2, J = 1/2).

Fig. 2. Breit-Rabi diagram for Au^{199} (I = 3/2, J = 1/2).

Fig. 3. Sketch of the shorted and terminated types of hairpins.

Fig. 4. Sketch of the K-band cavity hairpin.

Fig. 5. Standard transition resonance in Au^{199} at 6700 G.

Fig. 6. A $\Delta\nu$ transition resonance in Au^{198} at 0.89 G.

Fig. 7. Doublet-transition resonance in Au^{198} at 3214.5 G.

Fig. 8. Doublet-transition resonance in Au^{199} at 1047 G.

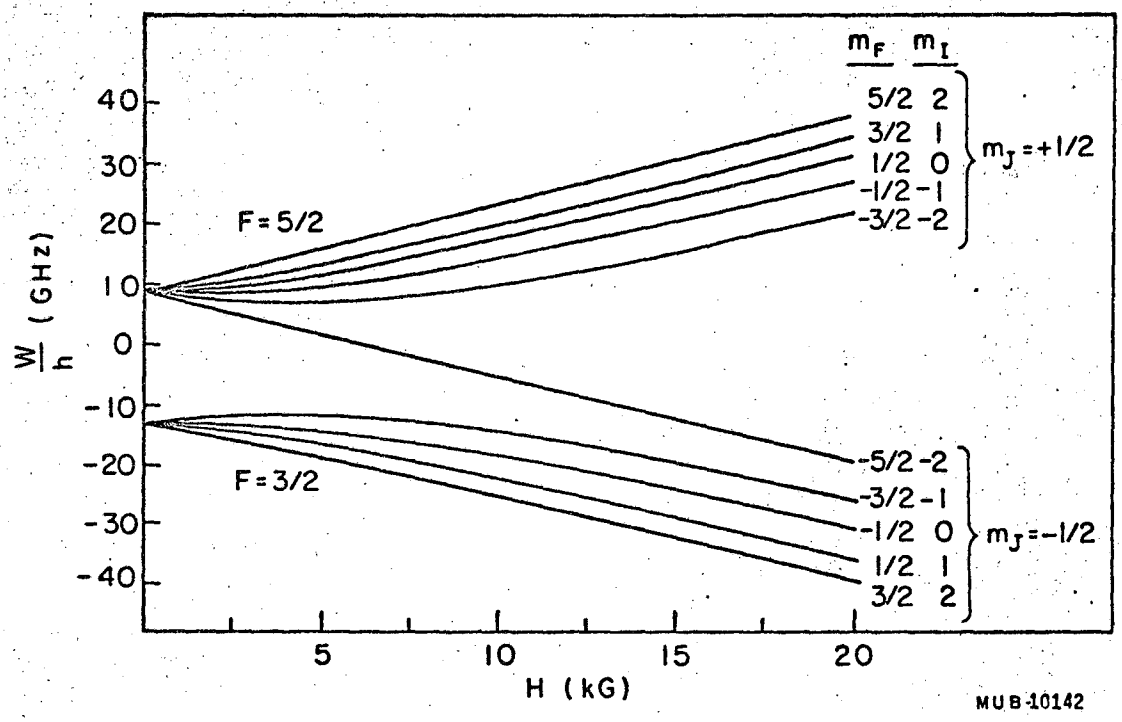
m_F m_I
5/2 2
3/2 1
1/2 0
-1/2 -1
-3/2 -2
m_J = +1/2
F = 5/2
-5/2 -2
-3/2 -1
-1/2 0
1/2 1
3/2 2
m_J = -1/2
F = 3/2
W/h (GHz)
40
30
20
10
0
-10
-20
-30
-40
5
10
15
20
H (kG)
MUB-10142

Fig. 1

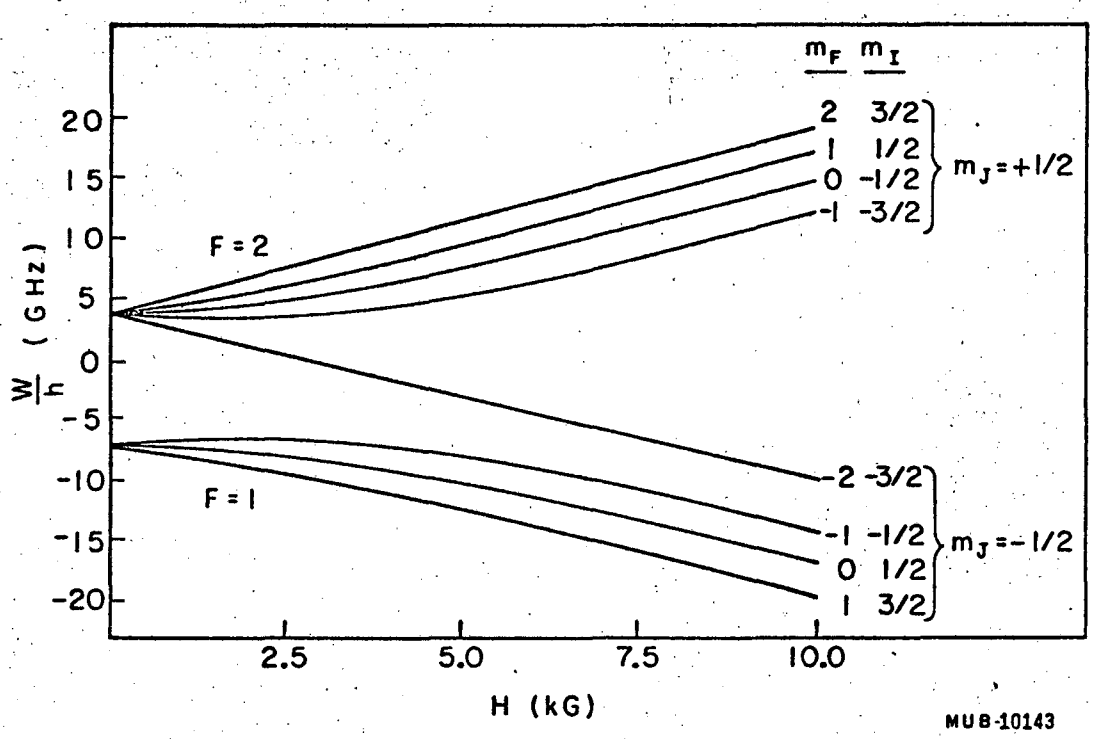
m_F m_I
2 3/2
1 1/2
0 -1/2
-1 -3/2
m_J=+1/2
F=2
F=1
-2 -3/2
-1 -1/2
0 1/2
1 3/2
m_J=-1/2
20
15
10
5
0
-5
-10
-15
-20
$\frac{W}{h}$ (GHz)
2.5
5.0
7.5
10.0
H (kG)
MUB-10143

Fig. 2

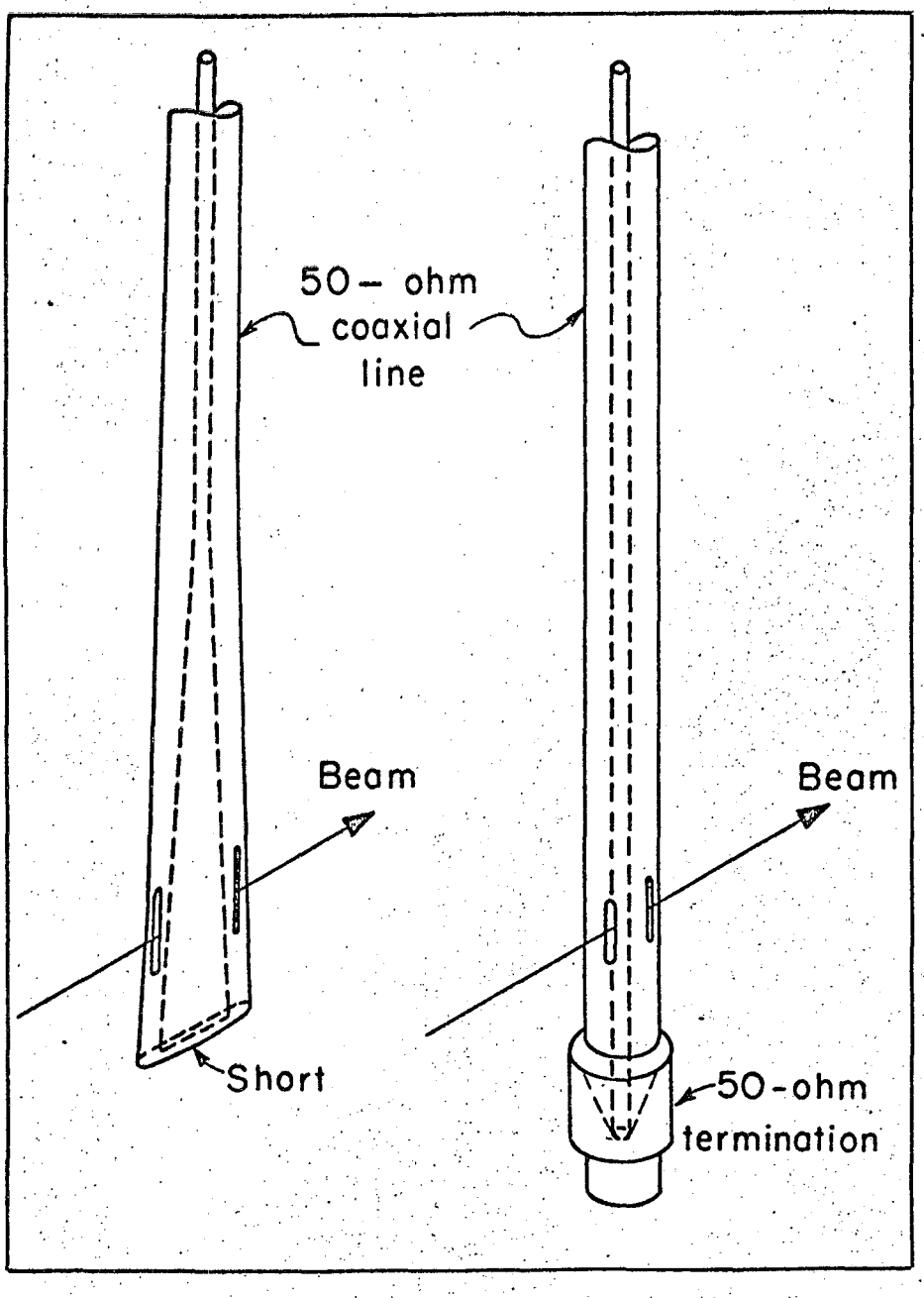
50 – ohm
coaxial
line
Beam
Beam
Short
50-ohm
termination
MUB4740

Fig. 3

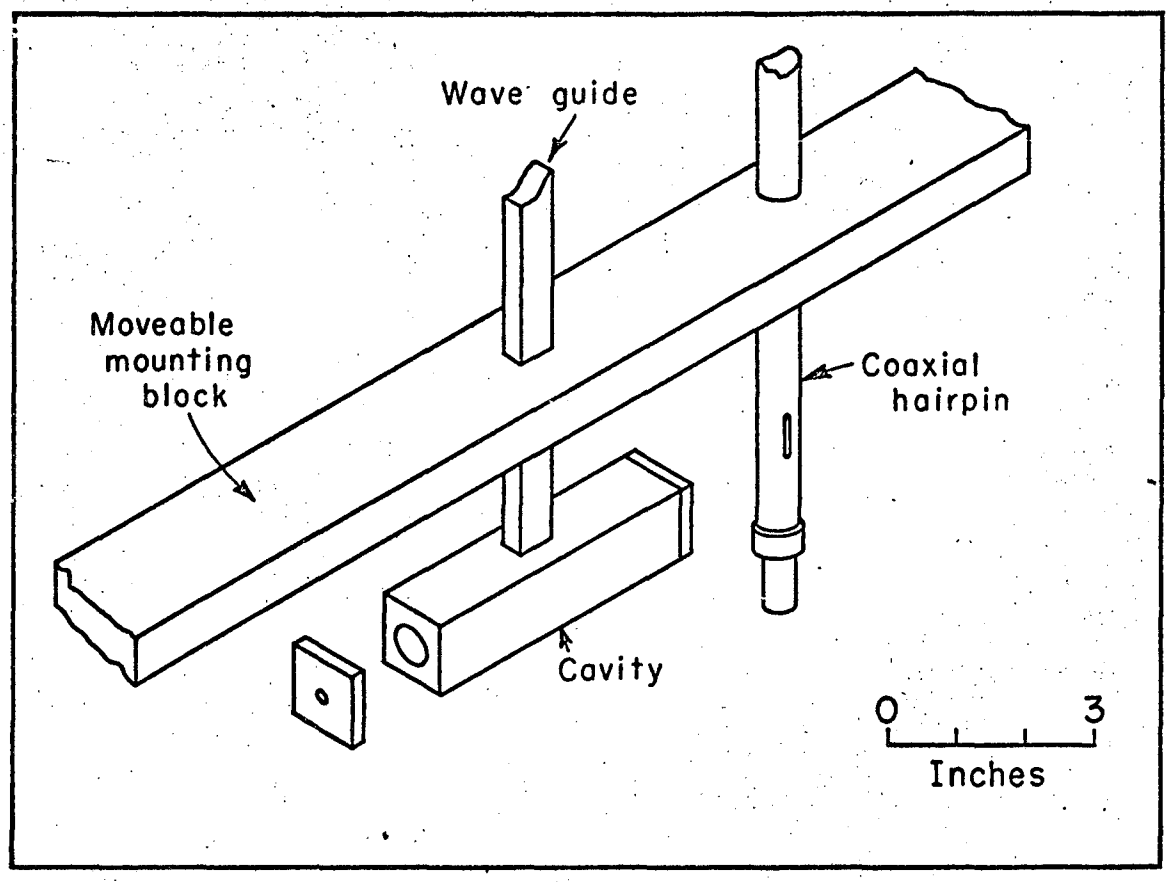

MUB-10038

Fig. 4

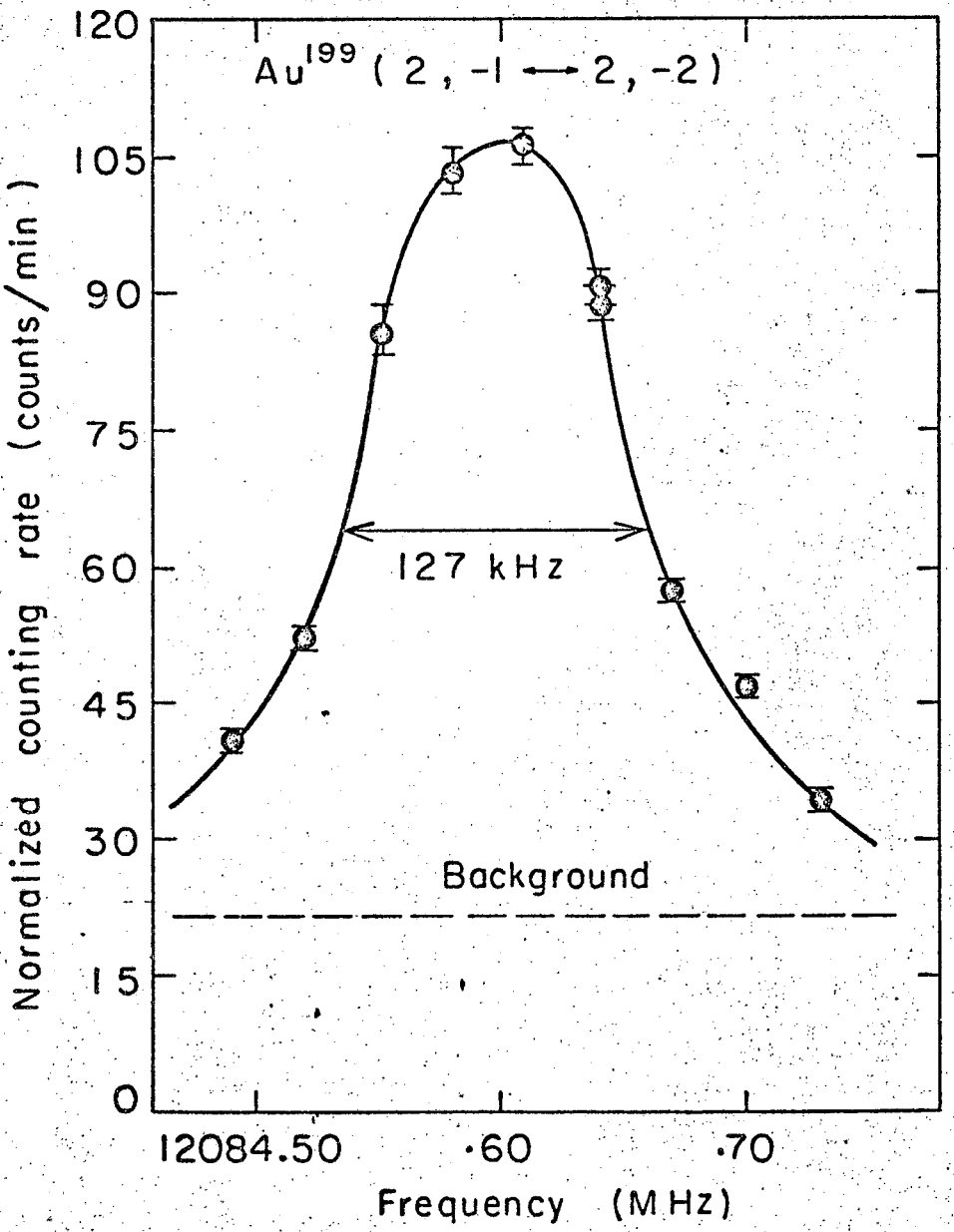

Fig. 5

MUB-10160

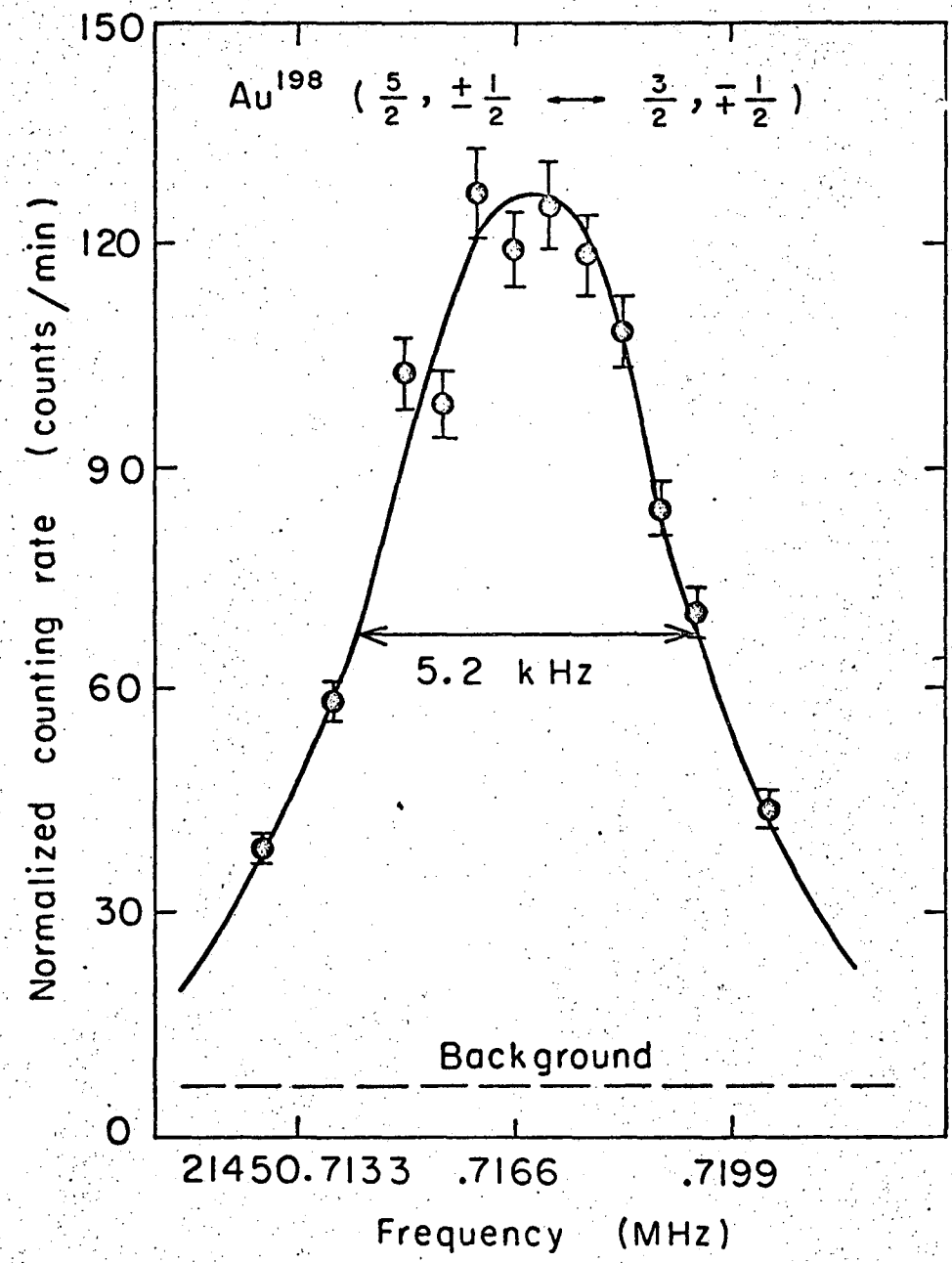

Fig. 6

MUB-10159

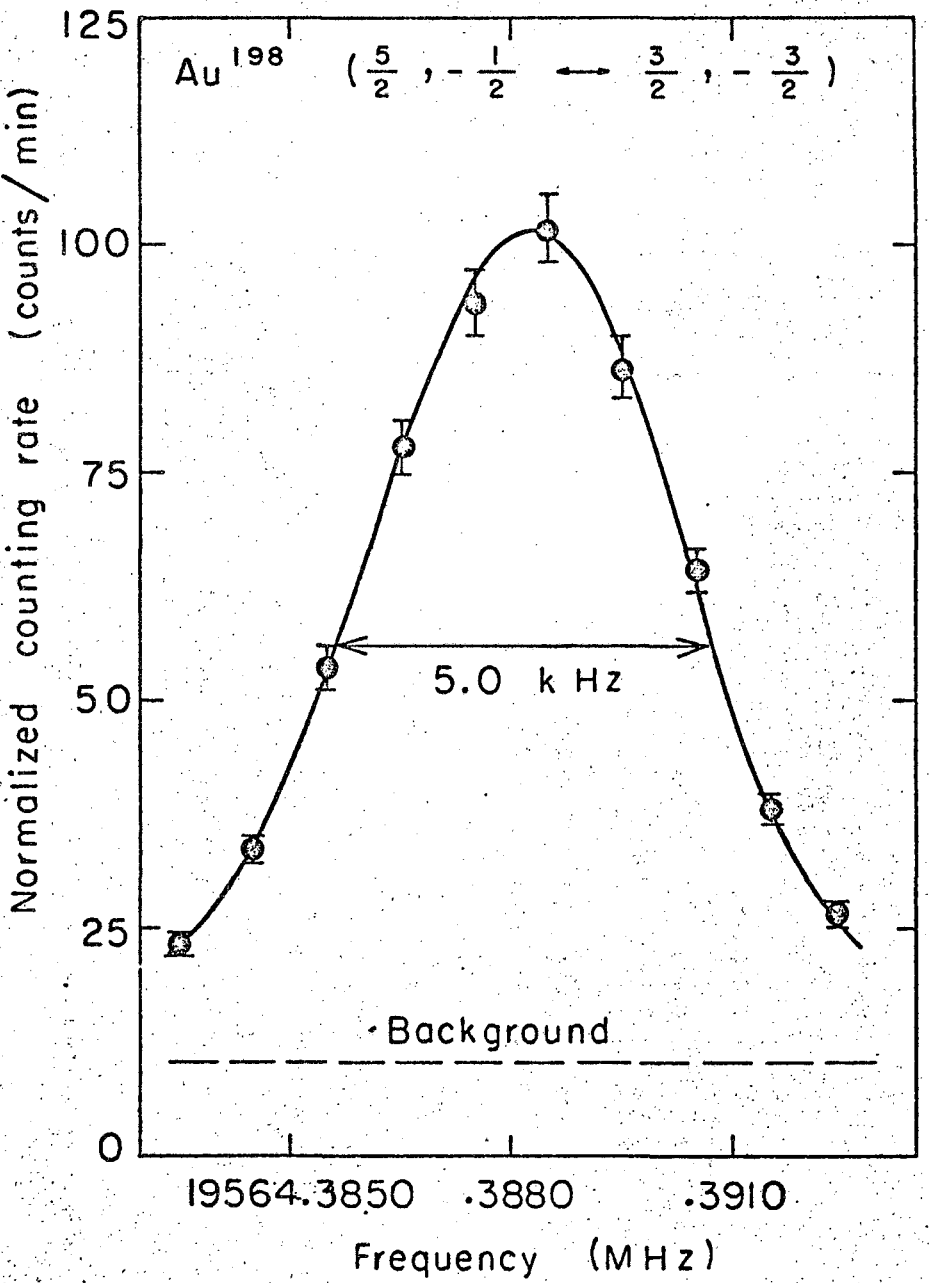

Fig. 7

MUB-10158

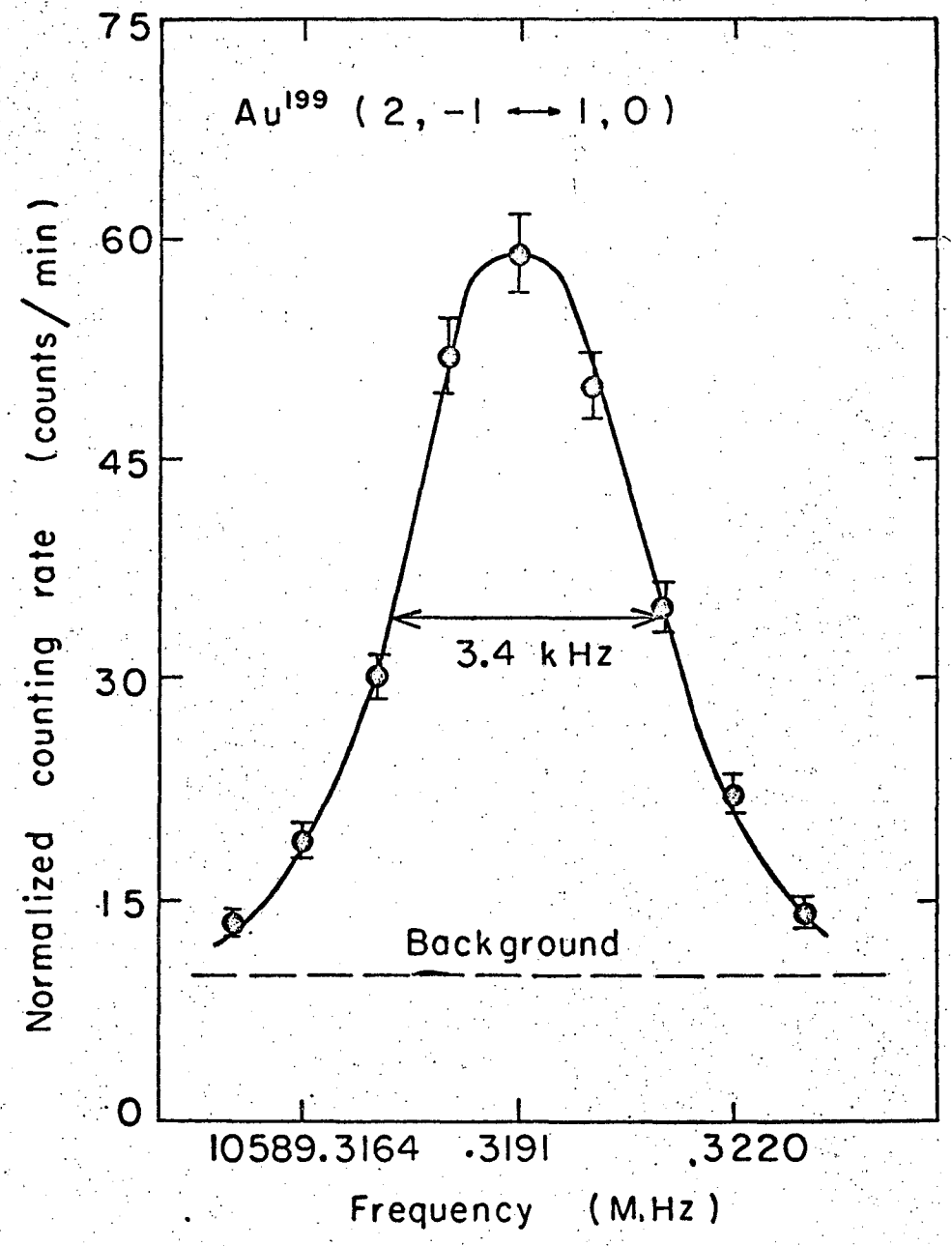

Fig. 8 MUB-10161